CHEMISTRY OF MATERIALS
Article

Chem. Mater. **2010,** *22,* 5905–5911 5905
DOI:10.1021/cm101824d

Investigation of the Chromic Phase Transition of $CuMo_{0.9}W_{0.1}O_4$ Induced by Surface Protonation

M. Gaudon,* C. Riml, A. Turpain, C. Labrugère, and M.H. Delville

CNRS, Université de Bordeaux, ICMCB, 87 avenue du Dr. A. Schweitzer, Pessac F-33608, France

Received June 30, 2010. Revised Manuscript Received September 28, 2010

$CuMo0_{.9}W_{0.1}O_4$ oxide is known to exhibit two allotropic forms (α and γ forms) linked by a first-order phase transition that can be induced by pressure and/or temperature. In this work, we show that this α → γ phase transition (with a chromic effect from green to brown color) can also take place at 25 °C by a simple immersion of the powder in an aqueous solution with acidic pH. This chromic phase transition from the high-temperature/low pressure form into the low-temperature/high-pressure form is shown to be induced by surface protonation, whereas the copper-molybdate powder is dispersed in acidic solutions. Wettability measurements on both phases were performed in order to confirm the affinity of the α-form for protons in comparison with the γ-form. Then pH metric titration (addition step by step of an acid solution on the powder, controlling at each step the pH evolution) has allowed describing the kinetic aspects of the surface protonation (kinetic laws were approached and discussed). Finally, an interpretative model of the "halochromic" phenomenon based on the modification of the cations environment at the liquid−solid interface was proposed. For the first time, a superficial interaction between a solid oxide and a liquid medium, for which no partial dissolution−recrystallization sequence is occurring, is shown to be sufficient for producing a phase transition of the whole oxide bulk.

Introduction

A thermochromic substance changes its color when subjected to a temperature variation in a certain range; a piezochromic substance changes its color under pressure.[1−3] The $CuMo_{0.9}W_{0.1}O_4$ oxide is one of the rare materials that exhibits these two properties. It crystallizes in two polymorphs, i.e., a high temperature−low pressure form (α-form with green coloration) and a low temperature−high pressure one (γ-form with reddish brown coloration). At ambient pressure, the γ → α phase transition occurs by heating at 85 °C, whereas the reverse one (α → γ) occurs by cooling at about −20 °C. Hence, the two polymorphic forms are stable at room temperature.[4−11]

In the present work, we show that this α → γ phase transition (with a chromic effect from green to red color) can also take place at 25 °C by a simple immersion of the powder in an aqueous solution with acidic pH.

In a first part, the wettability of the α-form was shown to slightly increase with decreasing the pH, and a solution in which the α-form is dispersed gets a pH increasing higher than the same solution in which the γ-form is dispersed. These experiments show a particular affinity of the α-form for protons. In a second part, the pH metric titration (step-by-step addition of an acid solution on the powder, controlling the pH evolution at each step) was found to be a key experiment for describing the phenomenon. The variation of the α → γ phase transition was shown to be directly controlled by the pH solution. Hence, the $CuMo_{0.9}W_{0.1}O_4$ oxide exhibits halochromic-like properties. Even if in literature, numerous organic dyes exhibit halochromic behavior (color controlled via solution pH),[12−18] such a property has never been reported before for inorganic oxides. Kinetic behavior of

*Corresponding author. E-mail: gaudon@icmcb-bordeaux.cnrs.fr.

(1) Nassau, K. *The Physics and Chemistry of Colour: The Fifteen Causes of Colours*;John Wiley and Sons: New York, 1983.
(2) Day, J. H. *Chem. Rev.* **1968**, *68*, 649–657.
(3) Gaudon, M. Thermochromic metal oxides. In *Chromic Materials, Phenomena and their Technological Applications*; Somani, P. R., Ed.; Applied Science Innovations : Maharashtra, India, 2010; Chapter 7.
(4) Ehrenberg, H.; Weitzel, H.; Paulus, H.; Wiesmann, M.; Wltschek, G.; Geselle, M.; Fuess, H. *J. Phys. Chem. Solids* **1997**, *58*, 153.
(5) Wiesmann, M.; Ehrenberg, H.; Miehe, G.; Peun, T.; Weitzel, H.; Fuess, H. *J. Solid State Chem.* **1997**, *32*, 88.
(6) Hernández, D.; Rodríguez, F.; Garcia-Jaca, J.; Ehrenberg, H.; Weitzel, H. *Phys. Rev. B* **1999**, *265*, 181.
(7) Gaudon, M.; Basly, B.; Fauque, Y.; Majimel, J.; Delville, M. H. *Inorg. Chem.* **2009**, *48*, 2136.
(8) Gaudon, M.; Thiry, A. E.; Largeteau, A.; Deniard, P.; Jobic, S.; Majimel, J.; Demourgues, A. *Inorg. Chem.* **2008**, *47*, 2404.
(9) Gaudon, M.; Carbonera, C.; Thiry, A. E.; Demourgues, A.; Deniard, P.; Payen, C.; Létard, J. F.; Jobic, S. *Inorg. Chem.* **2007**, *46*, 10200.
(10) Gaudon, M.; Deniard, P.; Demourgues, A.; Thiry, A. E.; Carbonera, C.; Le Nestour, A. L.; Largeteau, A.; Jobic, S. *Adv. Mater.* **2007**, *19*, 3517.
(11) Thiry, A. E.; Gaudon, M.; Payen, C.; Daro, N.; Létard, J. F.; Gorsse, S.; Jobic, S. *Chem. Mater.* **2008**, *20*, 2075.
(12) Anderson, L. C.; Gooding, C. M. *J. Am. Chem. Soc.* **1935**, *57*, 999.
(13) Anderson, L. C. *J. Am. Chem. Soc.* **1935**, *55*, 2094–2098.
(14) Thirumurugan, P.; Muralidharan, D.; Perumal, P. T. *Dyes Pigm.* **2009**, *81*, 245–253.
(15) Jaung, J.-Y. *Dyes Pigm.* **2006**, *71*, 245–250.
(16) Jung, Y.-S.; Jaung, J.-Y. *Dyes Pigm.* **2005**, *65*, 205–209.
(17) Koh, J.; Greaves, A. J.; Kim, J. P. *Dyes Pigm.* **2003**, *56*, 69–81.
(18) Reichardt, C. *Chem. Soc. Rev.* **1992**, *21*, 147–53.

Published on Web 10/12/2010

the protonation reaction was also characterized and interpreted. Finally, an explicative model of the new phenomenon is proposed.

Experimental Section

The starting γ-$CuMo_{0.9}W_{0.1}O_4$ powder is produced by a conventional solid-state route at 700 °C under air followed by a mechanical grinding.[8−11]

According to preliminary studies, the IEP isoelectric point of the α and γ phases is about 5. The starting pH of the aqueous solution for the surface titration of the two allotropic forms was chosen to be adjusted at 5. For all the titration experiments, 1 g of powder was immerged in pH 5 aqueous solutions in which about 1×10^{-5} M HCl was added in order to adjust the starting pH. The surface titration was made only for the acidic branch by adding step by step a 0.1 M HCl aqueous solution. Special care was taken to make sure of the stabilization of the pH of the mixture in between two successive additions of 1 mL of 0.1 M HCl aqueous solution. For extraction of the kinetic parameters, the pH variation was recorded until it stabilized after each 0.1 M HCl aqueous solution addition. The titration allows the access to the powder surface charge versus the solution pH according to the equation

$$\sigma = F/AV_{sol}([OH^-]_{solution} - [OH^-]_{initial} - C_{OH-} + C_{H+} - [H^+]_{solution} + [H^+]_{initial}) \quad (1)$$

where σ is powder surface charge density (C m^{-2}), F is Faraday constant (C mol^{-1}), A is powder surface area (m^2), $[OH^-]_{initial}$ and $[H^+]_{initial}$ are the respective concentrations in the starting solution, $[OH^-]_{solution}$ and $[H^+]_{solution}$ are concentrations measured during the titration, $C_{OH}{}^-$ and $C_H{}^+$ are the theoretical hydroxide/proton concentrations in the solution considering no interaction with the powder surface, and V_{sol} is the suspension volume. The apparatus used after calibration for these experiments is a Eutech Instruments pH 510 pH-meter equipped with Mettler Toledo InLabRoutine electrodes.

For wettability measurements, the powder was fixed at the bottom of a quartz capillary (∅ = 1.3 cm) equipped with a liquid-permeable film for sustaining the powder. The capillary is fixed so that the permeable film is placed just in contact with the aqueous solution. The capillary increase of the solution inside the sustained powder versus time inside the powder volume is determined with a 1×10^{-4} g balance. The penetration velocity into the powder, m^2/t ($kg^2\ s^{-1}$), the liquid viscosity, μ (Pa s), the liquid density, ρ_L (kg m^{-3}), the liquid superficial tension, γ_L (N m^{-1}), and the contact angle between the powder and the liquid, θ (°), characteristic of the wettability of the powder by the solution are linked by the Washburn law, where c is a negative constant linked to the powder morphology

$$m^2t^{-1} = c\gamma_L\rho_L\cos\theta/\mu \quad (2)$$

Hence, for a liquid with positive wettability ($\theta > 90°$), the $m^2 = f(t)$ function is a linear law with a positive slope proportional to the affinity of the powder for the liquid solution.

Powder X-ray diffraction patterns were recorded on a Philips PW 1820 apparatus equipped with a $K\alpha_1/K\alpha_2$ source and a copper anticathode. Diffraction patterns were collected with a 2θ step of 0.02° with a counting time of 10s per step in routine mode or, for more advanced investigations, with a 2θ step of 0.008° with a counting time over 200 s per step. The powder was carefully prepared (only deposited on aluminum substrate) in order to not modify the alpha-gamma ratio. The quantification of the alpha-gamma ratio was estimated from the main peak intensity of each form.

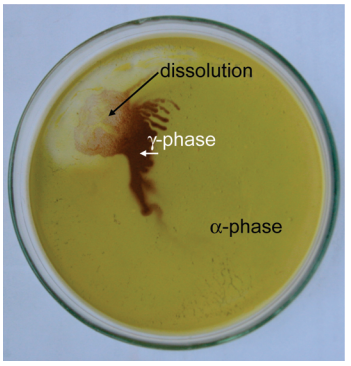

Figure 1. Effect of the addition of an HCl droplet on the $CuMo_{0.9}W_{0.1}O_4$ α-form. On the spot of maximum concentration of the acid, the powder dissolution can be seen. The dissolution seems to be preceded by a α-form → γ-form phase transition.

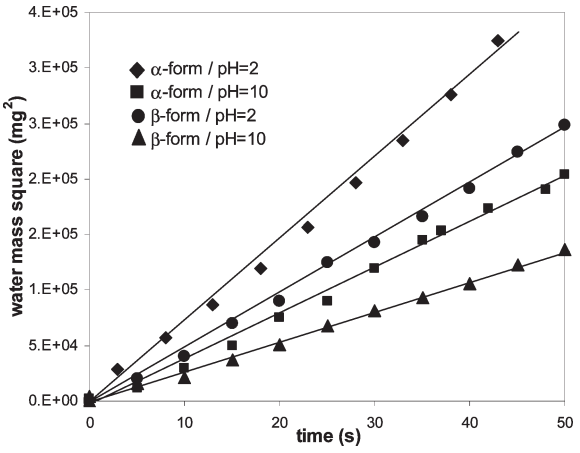

Figure 2. Wettability measurements of aqueous solution with various pH solutions on α-form and γ-form.

Transmission electronic microscopy (TEM) was performed on TECNAI F20 equipment with a field emissive gun, operating at 200 kV and with a point resolution of 0.24 nm. Diffuse reflectance spectra $R(\lambda)$ were recorded at room temperature from 350 to 850 nm with a step of 1 nm and a bandwidth of 2 nm on a Cary 17 spectrophotometer using an integration sphere. Halon was used as white reference for the blank.

Semiquantitative analyses can be performed from the area integration of the XPS pattern peaks. The spectrometer used is a VG/ESCALAB 220-iXL working with a MgK_α X-ray source. The XPS chamber gets a 1×10^{-10} mbar pressure. The angle between the X-ray source and the analyzed sample is 45° in order the analyzed depth is 3−5 nm.

Results and Discussion

Halochromism Phenomenon Investigation. The effect of an addition of an acidic solution droplet (1×10^{-1} M HCl) on the $CuMo_{0.9}W_{0.1}O_4$ α-form powder is illustrated in Figure 1. The impressive effect comes from the colored marking of the solution flow before its evaporation. Indeed, such acidic solution transforms the green α-form into the reddish brown γ-one in a few tens of seconds, and dissolution of the powder starts to occur at longer times.

Thus, Figure 1 immediately supports the occurrence of a double effect of a proton-rich aqueous solution of the green α-powder: first the phase transition occurs then followed by powder dissolution. The interaction between protons and the α-form leading to the $\alpha \rightarrow \gamma$ phase transition can be shown by wettability measurements. Two extreme pH solutions (pH 2 and pH 10) were tested on both allotropic forms. The results of the wettability experiments are reported in Figure 2.

One can see from the reported $m^2 = f(t)$ curves that the acidic pH solutions get a largely higher dampening than the basic ones. Moreover, for a same pH, the α-form is more dampened than the γ-form, showing more H^+ or OH^- ions interactions with the α-surface than with the γ-form. This assessment can be confirmed by measuring the pH variation of an aqueous solution with starting pH 3, in which 250 mg of either allotropic forms are immerged. The results obtained on the two allotropic forms are compared in Figure 3.

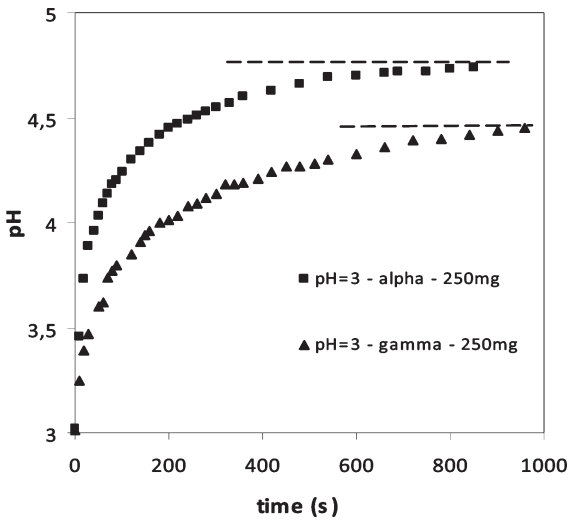

Figure 3. pH variation with time of aqueous solutions of starting pH 3 in which 250 mg of $CuMo_{0.9}W_{0.1}O_4$ powder (α- or γ-form) are dispersed.

The pH variation is larger (the amplitude between the asymptotic pH and the starting pH is wider) and the kinetic is faster (the pH asymptotic value is more quickly reached) for the α-form than for the γ-form. In brief, from these three experiments, it can be concluded that proton-rich solutions induce the $\alpha \rightarrow \gamma$ solid phase transition consequently to a large surface protonation of the α-form powder. When increasing the solution−powder contact time and/or decreasing the solution pH, i.e., increasing the acid attack conditions, the solid phase transition ends up in powder dissolution. The aim of the following studies is to determine whether the phase transition is a consequence of charge surface protonation only or results from a superficial dissolution of the powder occurring before the observed "macroscopic" dissolution.

In Figure 4 are compared the variations in the powder charge densities with the pH of aqueous solutions of starting pH 5 (100 mL) in which 250 mg of $CuMo_{0.9}W_{0.1}O_4$ powder of either α- or γ-forms are dispersed and an acidic solution (pH 1) is added step by step, 1 mL per 1 mL.

The charge density does not depend on the stirring nor on the presence of a supporting electrolyte such as NaCl. It seems to be only correlated to the suspension pH, and to increase while the pH increases. The isoelectric point being very close to 5 for both α- and γ-forms, the charge density increases are significant of the bonding of proton to free surface sites or of the substitution of hydroxyl groups present on the oxide surface. The charge density reaches a maximal value before a sharp decrease on only one pH unit. This decrease in the charge density can be explained by the superficial dissolution of the powder. The γ-form has a charge density maximal value about three times smaller than that of the α-form, showing that its surface is significantly less easily protonated than in the case of the α-form.

The introduction of NaCl as a supporting electrolyte clearly advantages the powder surface protonation. When the surface charge density increases, the presence of

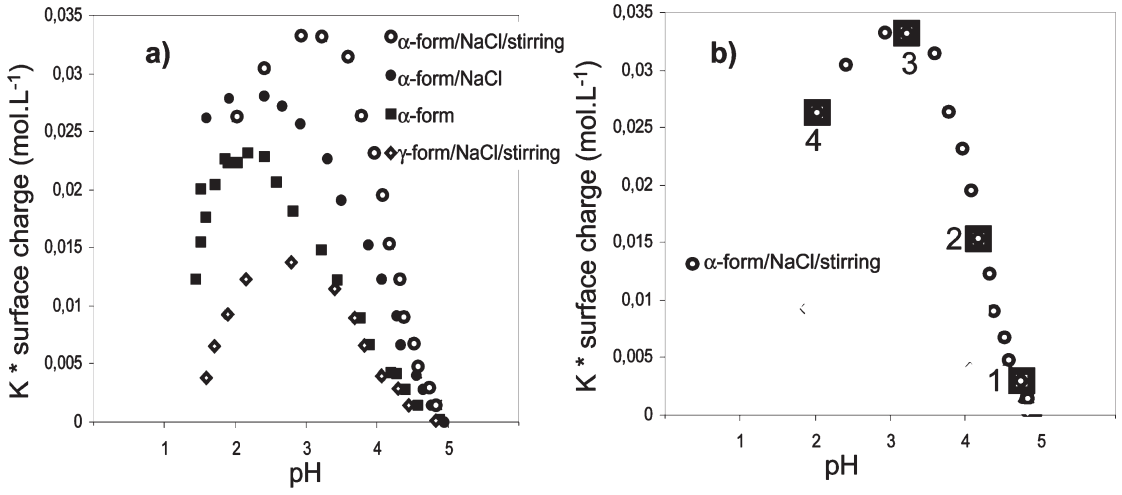

Figure 4. (a) Powder charge density evolution versus pH of an aqueous solution of starting pH 5 in which 250 mg of $CuMo_{0.9}W_{0.1}O_4$ powder (α- or γ-form) are dispersed and an acidic solution (pH 1) is added step by step. During the titration, the suspension can be highly stirred (◇, ○) or slightly stirred (■, ●), NaCl as electrolyte support can be added (●, ○, ◇) or not (■). (b) Focus on the powder charge density evolution versus pH of an aqueous solution of starting pH 5 in which 250 mg of $CuMo_{0.9}W_{0.1}O_4$ powder (α-form) is dispersed (with high stirring and NaCl addition conditions). Four addition steps are hereafter exploited and noted: step 1 (pH 4.8), step 2 (pH 4.2), step 3 (pH 3.2), and step 4 (pH 2.0).

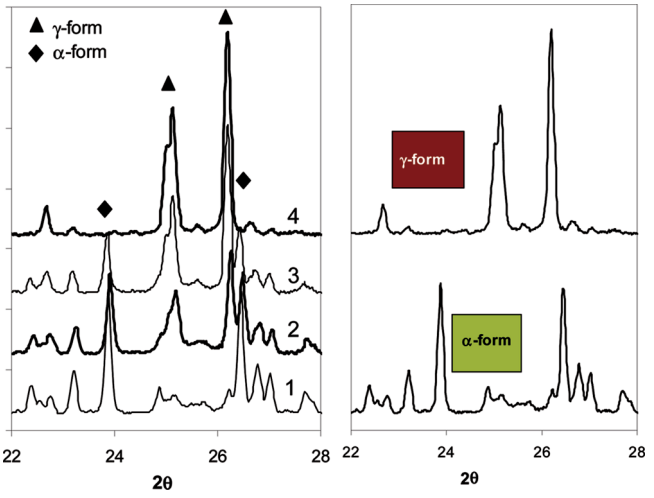

Figure 5. X-ray patterns of the powders extracted from the titration experiments at the steps 1, 2, 3 and 4, respectivel,y and comparison with α-and γ-pure allotropic form patterns.

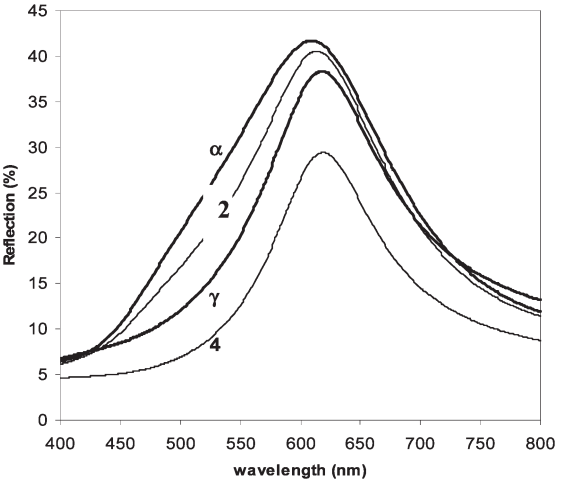

Figure 6. UV−vis diffuse reflection spectra performed on powders extracted from the titration experiments at the steps 2 and 4, and from pure α and γ forms.

a high density of positive charge clearly induces a screening effect and acts to the detriment of new protonation, due to the creation of a charge gradient from the powder surface to the solution. The stirring favors solution-powder contact and interactions: the charge density increases more abruptly, the maximal value is higher by 18% and takes place earlier for high stirring procedure than with a slow stirring one. As a consequence, the dissolution effect causing the decrease of the charge density also appears more quickly (for higher pH) with higher stirring rate. In Figure 4b, a focus on the powder charge density variation with the pH of the suspension, in which 250 mg of the powder green form is dispersed (using high stirring and NaCl addition conditions), is presented.

Four addition steps have been isolated and are hereafter exploited. Their X-ray powder diffraction patterns s are reported in Figure 5. From step 1 to step 4, i.e., when increasing the volume of acid solution, the peak intensities corresponding to the α-form decrease, whereas those of the peaks corresponding to the γ-one increase. Even for less than a unit pH variation (corresponding to step 2), far before the point of maximal charge density (corresponding roughly to step 3), the obtaining of a large amount of the γ-phase shows that the phase transition precedes the powder dissolution; definitively, the two phenomena are not convoluted. Actually, a mixture of about 50% of each allotropic form is already reached after step 2. This also can be shown by the colorimetric analyses reported in Figure 6. Comparing the reflection spectra of α-form, γ-form, and the mixture obtained at step 2, one can see that this mixture exhibits a reflectance roughly intermediate between the two pure forms. One can moreover notice that the powder obtained at step 4, after a partial dissolution, is darker than the γ-form: the reflective window centered at about 600 nm is less intense for the fourth step powder than for the pure γ-form.

Figure 7 presents the X-ray diffraction patterns of a pure γ-powder and the powder extracted on step 4 in which an internal NaCl standard for peaks intensity

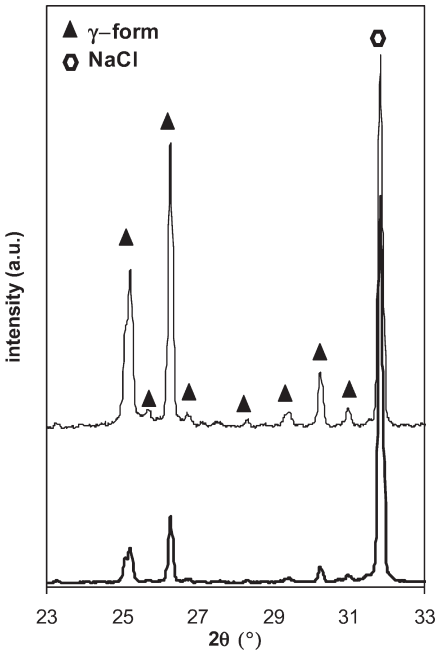

Figure 7. (a) X-ray diffraction of mixtures of the pure γ-form with NaCl and (b) the powder extracted from step 4 of titration; both mixtures contain 50 wt % NaCl.

calibration was added. This Figure shows after normalization of the NaCl main peak intensity that the fourth step powder exhibits a high quantity of an amorphous phase besides the crystallized γ-phase. Indeed, the γ-phase peaks of the mixtures are significantly reduced in intensity in comparison to the pure γ-powder.

The powder amorphization consecutive to its partial dissolution was found to come from a more selective attack on the surface copper cations than on the molybdenum/tungsten surface cations. Indeed, XPS spectra of a pure γ-powder and the fourth step powder (Figure 8) show a strong increase in the Mo^{6+}/Cu^{2+} peaks ratio between the two samples.

Hence, from the above results, it can be concluded that the powder phase transition occurs in slightly acidic conditions

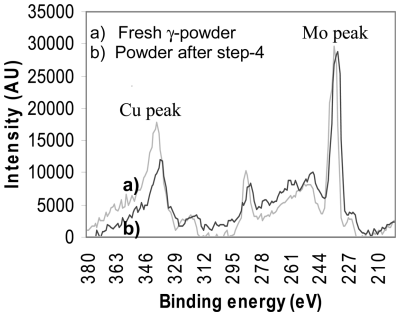

Figure 8. XPS spectra of (a) the fresh γ-form powder before acid titration and (b) the powder obtained after step 4.

which do not allow partial dissolution. The increase in the charge surface density is the only phenomenon responsible for the "halochromism" phenomenon observed here. For lower pH, a partial dissolution occurs and the solid powder then extracted is largely amorphous.

Grain Size Influence. The next experiments deal with the influence of the starting α-powder morphology on the phase transition advancement on step 2 (before any superficial dissolution is observed). To vary the starting morphology, we ground the powder in mechanosynthesis mortars. Three average crystallite sizes are compared: the raw powder synthesized at 700 °C (which is overmicrometric), the ground powder (submicrometric), and with an intermediate crystallite size, the ground powder postannealed at 600 °C (the sintering advancement degree being significantly lower at 600 °C than for 700 °C). The compounds exhibiting piezochromic phenomena, the grinding produces the transition from the green to the brown form. In order to recover the green high temperature form, before its immersion into acidic solution, the ground powder was heat up to 200 °C. Figure 9 shows the three X-ray diffraction patterns of the three powder samples after their immersion in a solution with a pH equivalent to the one reached at step 2. After normalization of the X-ray pattern intensities in order to get the same α-phase peak intensities, it can be observed that the γ-phase peak intensity, on which the illustration is focused, decreases drastically with the powder grain size reduction.

Hence, the cooperative phase transition that is favored for large grain sizes is now much more difficult to obtain as also observed by Ito et al; when they compared this phase transition for $CuMoO_4$ single crystals and powdered materials.[19] On the one hand, the last experiment definitively proves without any doubt that the particles partial dissolution is not at the origin of the phase transition, because such a decrease in the grain size would support a partial dissolution effect and thus, the $\alpha \rightarrow \gamma$ phase transformation which is not the case. However, the surface/volume ratio increasing while the grain size decreases, it is getting difficult to explain why a phase transition occurring from a surface protonation of the particles is disadvantaged by a grain size reduction. It has to be here referred to another series of experiments

(19) Ito, T.; Takagi, H.; Asano, T. *Chem. Mater.* **2009**, *21*, 3376.

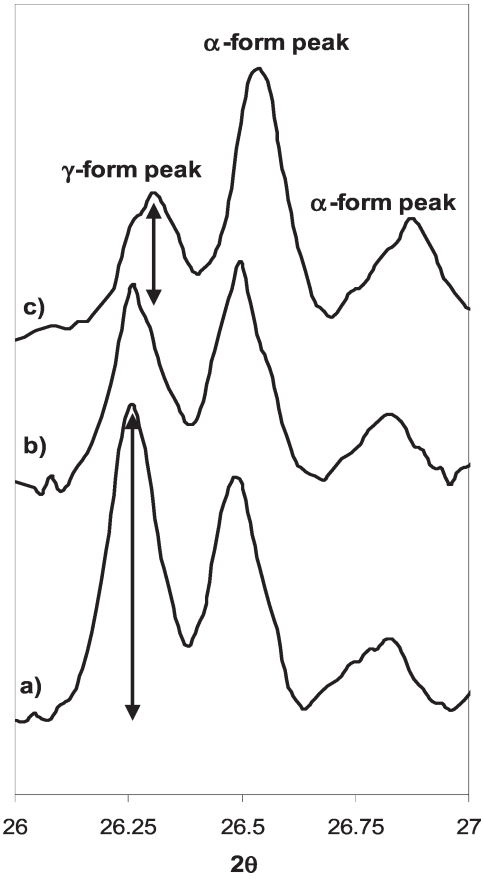

Figure 9. X-ray patterns performed on powder extracted from the titration experiments at step 2 on (a) raw powder (synthesized at 700 °C), (b) ground powder postannealed at 600 °C, (c) ground powder, respectively.

performed on the $CuMo_{1-x}W_xO_4$ powder. Indeed, as already shown in literature in some of our previous studies,[8,10] the copper molybdate powder exhibits a piezochromic transition from green to red phase ; for a same composition, i.e. a same tungsten concentration, the pressure to apply on the powder in order to achieve the phase transition increases with the particle size reduction. Furthermore, a size reduction below a critical value of the crystallite diameter definitively stabilizes the α-form, i.e., it prevents the high-temperature form from the thermochromic $\alpha \rightarrow \gamma$ phase transition via a temperature cooling down. This piezochromism phenomenon dependence versus particle size and the definitive stabilization of the α-form below a critical particle size can also be directly correlated to the halochromism phenomenon.

Kinetic Study. The last part of the study concerns the determination of the protonation kinetic laws and their variation with time at different steps of the acid addition. Figure 10 presents the pH variation curves in % (considering 100% of pH variation is reached in first approximation after 40 min.) versus the postaddition time for steps 1, 2, 3 as identified previously of the acid titration.

The kinetic of protonation is strongly shifted downward with the advancement degree of the titration. The stabilization of the pH is faster in slightly acidic conditions than in more acid solutions. The protonation reaction of a

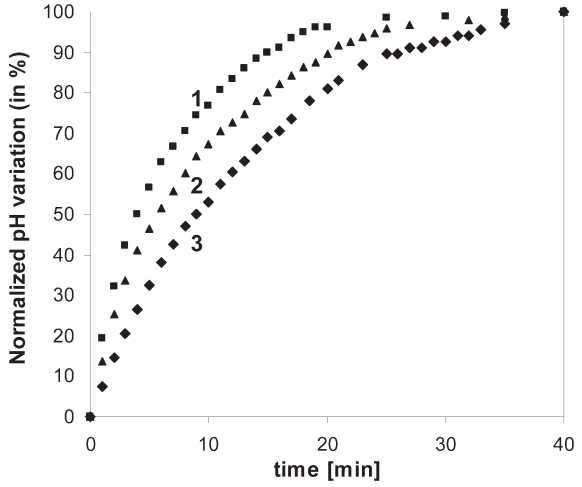

Figure 10. pH variation versus post addition time for titration step1 (pH 4.8), step2 (pH 4.2), step3 (pH 3.2).

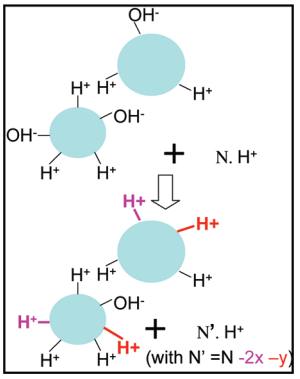

Figure 11. Representation of the powder surface protonation produced by an additional addition of the HCl (1×10^{-1} M) solution on the powder dispersion.

powder dispersed in an acid solution (in which the presence of OH^- hydroxyl ion has been taken into account, this presence should be neglected in comparison to the H^+ ions quantity) is schematized in Figure 11

For the protonation reaction, one goal of the kinetic study is to know if the surface powder sites susceptible to be protonated are in large excess or not in comparison to the effective number of sites protonated after each addition. The kinetic variation at different solution pHs was performed on the same powder quantity (powder area). The quantity of proton reacting at each step can be easily evaluated from the pH variation occurring for each acid solution addition. One can notice that the proton can occupy a new surface site or substitute one hydroxyl group. As shown in Figure 11, the substitution of one hydroxyl consumes two protons in solution, whereas the surface absorption on a new site consumes only one proton in solution. Considering that the total variation of the pH only leads to the whole quantity of protons (ΔH^+) disappearing during the protonation reaction, in first approximation, the ΔH^+ was taken as the reactant quantity. The protonation rate can be obtained from the equation

$$v_t = d[\Delta H^+]/dt = k[\Delta H^+]^{\alpha}$$

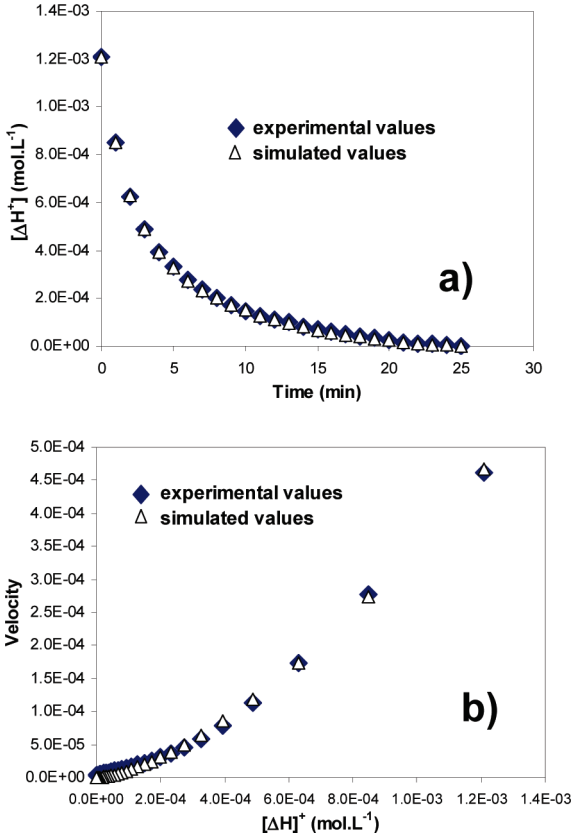

Figure 12. (a) Variation in $\Delta H^+ = [H]^+$ at time $t - [H]^+$ at the end of the protonation (difference of concentration between the $[H^+]$ concentration at time t and the $[H^+]$ final concentration reached at the equilibrium at the stage 2 of the titration)during equilibration time. (b) Velocity of the protonation versus the concentration difference in the solution (ΔH^+).

with $[\Delta H^+] = 10^{-pHt} - 10^{-pHa}$, where pH$t$ is the pH at a time t during the pH variation produced by the acid solution addition and pHa is the pH asymptotically reached after the addition. First, the $[\Delta H^+]$ curve versus time after addition was plotted and fitted with the most appropriate function: the chosen function is an exponential decay of second order

$$[\Delta H^+] = A_1 \exp(-t/t_1) + A_2 \exp(-t/t_2) + \Delta H_0$$

with three free parameters, t_1, t_2, and ΔH_0, this latter representing the whole quantity of proton reacting at each acid addition step. An illustration for the dependence obtained after step 2 is reported in Figure 12a.

To get the kinetic law, we differentiated this reaction such as the characteristic kinetic velocity can be expressed as

$$\begin{aligned} v_t &= d[\Delta H^+]/dt \\ &= -t_1 A_1 \exp(-t/t_1) - t_2 A_2 \exp(-t/t_2) + \Delta H_0 \end{aligned}$$

The simulated velocity variation versus the ΔH^+ reactant concentration was then fitted by the equation $v_t = k[\Delta H^+]^{\alpha}$, where α represents the partial reaction order on the considered reactant and k is a pseudoconstant involving possible other limiting reactants as powder surface sites. An illustration for the dependence of the velocity versus obtained ΔH^+ for step 2 is reported in Figure 12b.

For step 1, step 2, and step 3, respectively, the fitted partial reaction orders are 1.55, 1.51, and 1.34, the fitted k values are 54, 12, and 1.2 in $mol^{1-\alpha} L^{\alpha-1} min^{-1}$. As can be seen, both reaction orders and pseudoconstant rates vary depending on pH. Especially the k values show strong differences, which imply the dependence on other factors than the quantity of the considered reactant: ΔH^+ concentration. The decrease of the reaction order in step 3 depends not only on this screening effect but also on the beginning of the partial dissolution of the copper cation. Our interpretation of the strong decrease of the k value with the advancement of the protonation is the occurrence of a screening effect due to the positive charging of the surface.

The above interpretation is also confirmed by the very low k value obtained for step 1 ($k = 2.5\ mol^{1-\alpha} L^{\alpha-1} min^{-1}$) when no NaCl supporting electrolyte is used because the screening effect is then drastically increased.

Eventually, the fitting of α partial orders superior to 1 can be interpreted as the appearance of a stronger screening effect "during" pH stabilization after each addition. Hence, the slight decrease of the partial order with the protonation advancement should be explained as a less and less important relative evolution of the screening effect during the pH stabilization versus the surface protonation advancement.

Proposed Interpretative Model. It was shown in this paper that the protonation of the surface of the α-form of the $CuMo_{0.9}W_{0.1}O_4$ oxide leads to its phase transition into the γ-allotropic form. The phase transition does concern not only a thin layer on the grain size surface but the entire grain volume. This shows a rapid domino-propagation of the phase transition from the grain surface to the whole bulk. The quick domino propagation can be explained by the large cell parameters variation between the two allotropic forms (cell volume difference between the two allotropic forms is about 11%). There is a too large misfit between the two α- and γ-phase crystallographic networks to imagine the occurrence of stable interface boundaries. The progressive character of the phase transition versus the advancement of the surface protonation can be explained only by the dependence of the phase transition critical point on the crystallite size. It was shown here that the smaller are the particle sizes, the more stable is the green α-phase. Eventually, one can propose a surface mechanism explaining the "motor" driving force of the phase transformation. A proposed interpretation is based on bond valence considerations as illustrated in Figure 13. Let us take into consideration the surface tetrahedral sites (one face corresponding to the surface section) in which the bond valences of the Mo−O bonds are all relaxed and near their equilibrium value: 1.5 (corresponding to the molybdenum oxidation degree value divided by the engaged bonds number around the Mo^{6+} cation). The protonation of the three surface oxygen anions, whether one considers bridging protons or terminal ones, leads to a strong decrease of the bond valences of the three concerned Mo−O bonds in order to keep a stable valence for the oxygen anions. This bond

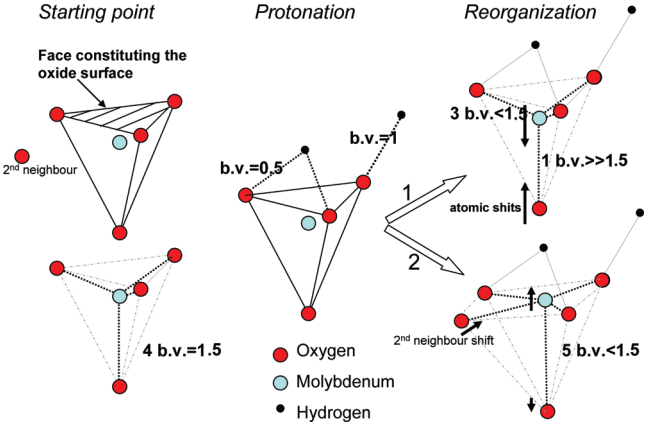

Figure 13. Schematic illustration of the stabilization of octahedral sites instead of tetrahedral sites in the oxide surface consecutive to the protonation of some oxygen atoms. b.v. is used for bond valence. The protonation induces a diminution of the b.v. of the concerned oxygen−molybdenum bonds. The reorganization could imply strong atomic shifts to keep the tetrahedral Mo^{6+} coordination or an increase in the Mo^{6+} coordination.

valence decrease can be relaxed by a strong shift of the molybdenum cation far from the surface or by a reorganization of the tetrahedral sites into octahedral ones (or at least, as shown in Figure 13, into truncated octahedral sites, i.e., square plan pyramidal sites) for which the average Mo−O bond value is close to 1. Hence, the creation of O−H bonds on the surface anions tends to produce an increase in the surface cationic site coordination. This effect is sufficient to produce here the first "halochromic" mineral material observed because of the proximity of the reticular energy of the two-allotropic forms conferring a "metastable" character to the starting green α-powder.

Conclusion

The chromic phase transition from the high-temperature/low-pressure form of the $CuMo_{0.9}W_{0.1}O_4$ compound (γ-form, red-brown form) into the low-temperature/high pressure form (α green phase) can be induced by surface protonation, whereas the copper−molybdate powder is dispersed in slight acidic aqueous solutions.

Wettability measurements on both phases showed the affinity of the α-form for protons. The pH metric titration (addition step by step of an acid solution on the powder, controlling at each step the pH evolution), the kinetic aspects of the surface protonation showed that the protonation is effectively at the origin of the phase transition. Indeed, the $\alpha \rightarrow \gamma$ phase transition was shown to be directly controlled by the pH solution. A proposed explanation based on the bond-valence model for this 'halochromic" phenomenon could be the increase of the coordination sphere of the cations at the powder surface. It can then be proposed that the α-form that exhibits 4-coordinated Mo^{6+} cations seems thus destabilized at the surface proximity and tends to transform by a domino effect from grain surface to bulk (which can be explained easily from the large cell volume difference between the two allotropic forms) into the γ-form with Mo^{6+} octahedral sites.